Simulation of strain rate, material flow, and nugget shape during dissimilar friction stir processing of AA6061 aluminum alloy and Al-Mg$_2$Si composite

Nayak Himansu Sekhar Ray, Pradipta Kumar Rout
College of Engineering Bhubaneswar, BPUT, Odisha, India

Abstract

In order to investigate the visco-plastic material flow during friction stir welding of the AA6061 aluminum alloy and the Al-Mg2Si composite dissimilar junction, a three-dimensional model based on computational fluid dynamics (CFD) was created. Using the volume of fluid (VOF) approach, the dissimilar joint was modeled. The heat created by viscous dissipation was given a definition through the use of the volumetric equation. Three rotational speeds of 720, 920, and 1120 rpm were examined for the model. The nugget form was presentexcellent concordance with the relevant experimental findings. The outcomes demonstrated that the top surface of the workpiece and the shoulder's outside edge experienced greatest velocities and strain rates. Furthermore,the side that was progressing achieved the highest temperature. The rate of strain at the forward-moving side and the withdrawingside was roughly 926 s^{-1} and 975 s^{-1}, accordingly. In the stir zone's area where material mixing is predominant; the aluminum alloy AA6061 has a volume fraction of 0.4–0.8.

Introduction

Different joint applications have been developed as a result of the need for high-performance, lightweight, and affordable materials in various industrial domains, including the aerospace and automotive industries.The creation of high-quality couplings between an alloy and a metal matrix composite (MMC) is fascinating since composites can only be utilized in structural components where their characteristics improve performance while also lowering costs and weight.[1, 2].

Al-Mg2Si composites are appealing among particulate MMCs because of their excellent wear resistance, low density, and high strength to weight ratio. The Mg2Si reinforcing particles in these composites have a high melting temperature and a high hardness.At high temperatures, these particles can stop the grain boundary from slipping. As a result, Al-Mg2Si composites can be utilized in the fabrication of automotive and aeronautical components, including pistons and piston rings and brake disks [3]. Furthermore, wrought Al-Mg-Si alloys have a high strength and can be heat treated, such as AA6061. In addition to being used in automobile and

aircraft applications, AA 6061 aluminum alloy exhibits good potential for creating dissimilar joints with other materials [4].

Using fusion welding techniques to create the different junction has degradation of the welded structure. Intermetallic compound synthesis, segregation, the reinforcing phase's response, and a fusion welding flaws can be exemplified by coarse microstructure.These flaws can be removed with a solid state connecting technique like called FSW, or friction stir welding. As FSW is carried out beneath the solidus temperature of the components, the very audible differences in joints have been created between Al-Mg2Si and an aluminum alloy combination [5,6]. Using a spinning, non-consumable tool that is introduced into the joint interface and moved along it, FSW is a solid state welding process. The tool's two primary uses are (i) heat generating and (ii) material transportation. Friction between the tool and workpiece as well as metal deformation cause the heating. A junction is created when the material flows to the tool's trailing side due to tool movement caused by the material's softening effects from localized heating and temperature increases [7].

The mechanical characteristics and structural differences between joints made of 5083 and 6061 aluminum alloys were examined by Shigematsu et al. [8]. After examining the material's characteristics, they discovered that the dissimilar joint's strength is 60% of the base material and is comparable to the strength of similar joints. Wert [9] looked at the weld microstructure in friction stir welded joints made of AA2024 alloy and AA2014-20 vol% Al2O3 MMC in a different study. It was discovered that the final material flow pattern was influenced by the hardness of the materials. The parameters of the weld for one and two pass welds at the interface of the Al-Mg2Si composite and 2024-T4 aluminum alloy were investigated by Sharifitabar and Nami [5]. Their findings indicated thatthe material flow pattern was complex, and the tool's rotation at the stir zone (SZ) refined the Mg2Si particles. Huang and associates[10] examined the material flow of aluminum 6082-T6 at the FSW combine with the copper foil. Cu foil is employed as a material marker. Those found that the shoulder prevented materials from retreating primarily side (RS) to the advancing side (AS), and the pin's function is extrusion in the method. Silva and colleagues [11] examined the 2024-T3 material flow and the dissimilar joint 7075-T6. They discovered that SZ is more gradual at the RS and sharp at the AS. Additionally, they illustrated how a change in rotational speed affects the mixing of two materials. There has been limited material mixing at the low rotational speeds. In their investigation into the material flow and mechanical characteristics of 7075 and 2024 dissimilar joints, Alvarez et al. [12] discovered the same outcomes. Better weld appearance and ideal

mechanical properties were attained at low rotational speed, but mixing is constrained. It is possible to clearly see the onion ring pattern at the high rotational speed. Numerous experiments and mathematical models have been used to analyze the process since the creation of FSW. The spinning of the tool, the heating of the machinery, and the high strain rates make it challenging to keep an eye on the specifics of the process. Process modeling thus appears to be required for a deeper comprehension of it [13, 14]. The conservation equations of mass, momentum, and energy can be solved to provide a correct explanation of plastic flow and temperature fields. Recent years have seen a number of studies on the FSW process and simulation of dissimilar metals.

Using Fluent and computational fluid dynamics (CFD), Kishor et al. [15] created a two-dimensional thermal model for dissimilar joints of the aluminum alloys AA6061-AA5083 and AA2024-AA7075. They modeled the two-phase problem using the volume-of-fluid (VOF) model. They researched the production of heat as well as material flow for the three distinct pin profiles and material locations. They demonstrated how the highest temperature produced at the more durable substance. A CFD was used by Padmanaban et al. [16] model in addition to the VOF model for researching material and heat transfer flow of the dissimilar joints AA2024 and AA7075. They didn't think about the relative velocity formulas for the surrounding circumstances and described the walls as being in motion. They investigated the impact of each after measuring the rotational speed and welding velocity, it was discovered that the temperature distribution was asymmetric.In Liu et al.'s study [17], a coupled thermos mechanical model to investigate 6061 Al's dissimilar FSW combine with TRIP steel.

To simulate the multiple phase behavior, they employed the VOF method, Fluent software, and computational fluid dynamics. Their findings demonstrated that a frictional shear stress contact condition produced a material distribution that was significantly better than a velocity contact condition. The results of a three-dimensional heat generation simulation based on CFD during FSW of AISI A441 steel and aluminum alloy AA1100 were reported by Derazkola et al. [18] in a different study. Two volumetric heat equations were defined by them. The heat produced at the interface between the tool pin and the workpiece was defined by one of these equations, and the heat produced by viscous dissipation was defined by the other. This work makes use of the viscous heating equation. A finite element method (FEM)-based 3D thermal model for the dissimilar joint of the aluminum alloys AA5086 and AA6061 was created by Jamshidi Aval et al. [19]. Their findings demonstrated asymmetric heat generation in line with CFD-based simulations.

Despite similar joints, the literature review above shows that there are few research about the modeling of joining dissimilar metals by FSW and none about the simulation of FSW of AA6061 aluminum both Al-Mg2Si MMC and alloy. Consequently, numerical modeling of 3D

material flow of different AA6061 aluminum alloy during FSW and his study's primary focus is on Al-Mg2Si composite. Models of are carried out at three rotating speeds, with the findings documented in this piece.

2. Numerical modeling

To simulate material flow during dissimilar FSW of AA6061 aluminum alloy and Al-Mg2Si composite, a 3D model based on CFD has been created. As shown in Fig. 1, the computational domain consists of the workpiece, tool, and its dimensions in millimeters. There are roughly 440000 tetrahedron elements in the domain.Much smaller meshes are used in this area because of the steep gradient in strain rate and velocity close to the pin surface.The tool revolves at a steady pace in a counterclockwise direction. The term "inlet" refers to the surface at the positive x-axis, whereas "outlet" designates the surface across from it. From the intake to the output, the material flows at the domain at a welding velocity.
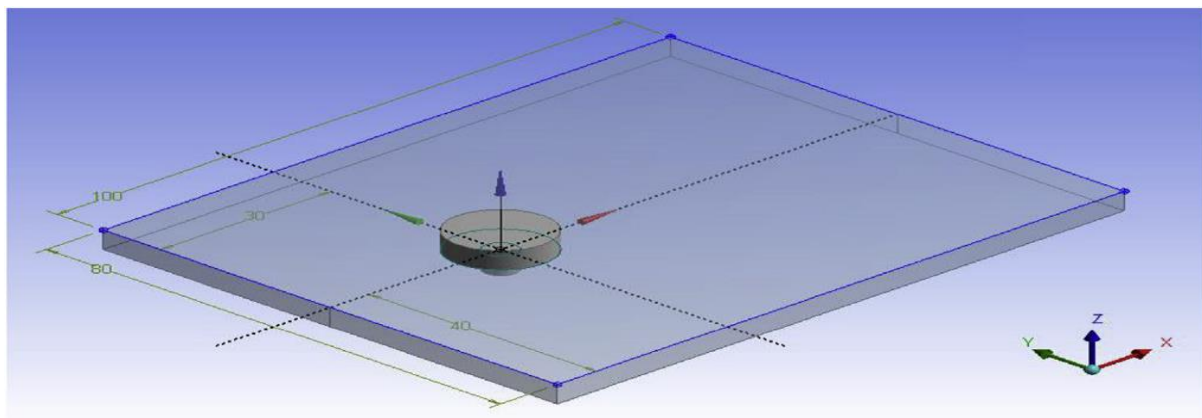

Fig. 1. Computational domain and its dimensions in mm.

When slip fraction (d) is expressed. t is the shear stress, u is the rotational speed, V is the welding velocity, m is the friction coefficient, and PT is the normal pressure, which is equal to 12.7 MPa based on the previous works [23]. The extent of d is between 0 and 1, and in this study, it is considered 0.65 according to the other simulation works [23]. Equations (7) and (8)

have defined the relative velocity at the contact area between the workpiece and the shoulder. Equations (9)e(11) have also been used to express the relative velocity between the workpiece and the pin periphery [24].

3. Experimental procedure

The FSW trials were carried out using Al-15 wt%Mg2Si in situ composite plates and AA6061 aluminum alloy plates that were 150 mm long, 100 mm broad, and 5 mm thick. Table 2 contains a list of the basis materials' compositions. The welding tool had a flat shoulder, a threaded cylindrical pin, and was constructed from H13 hot-work steel. The diameter of the pin was 5 mm, and the shoulder was 15 mm. The AS was covered with the Al-Mg2Si composite plate. The welding velocity was 0.002 m/s (120 mm/min), and the experiments were conducted at three different rotating speeds: 720, 920, and 1120 rpm.To examine the welded samples' macrostructure, the metallographic sections were ready**.** The samples were etched using a reagent composed of 6 mL HF, 6 mL HCl, 3 mL HNO3, and 150 mL H2O [36].

4. Results and discussion

Fig. 2 displays the 3D temperature distribution pattern. Because heat is supplied more quickly to the cold region in front of the tool than to the preheated region behind it, this pattern suggests that the temperature profiles are compressed ahead of the tool and expanded behind it. Fig. 3 depicts the temperature differences on the advancing and retreating sides. Temperature increases from 300 K at the workpiece's side surfaces to a maximum value on the pin surface gradually. At a rotational speed of 1120 rpm, the temperature at the RS (AA6061 aluminum alloy) and AS (Al-Mg2Si) reaches 887 K and 772 K, respectively [24].

The velocity vectors for each of the three rotational speeds at the workpiece's top surface and cross-section are displayed in Fig. 4.Because the impact of tool shoulder velocity as a source of momentum is most prominent in the upper half of the workpiece, the maximum velocity occurs at the top surface.The velocity values at three distinct values of z are displayed in Fig. 5. Because the value of ur is highest at the outer edge of the shoulder, it is observed that this is the location where the maximum velocity is reached. At the outer edge of the shoulder, the maximum velocities at 720, 920, and 1120 rpm are approximately 0.42, 0.424, and 0.516 m/s, respectively. The velocities rapidly reach to zero at the tool pin surface.

The calculated strain rate and viscosity at the top surface of the workpiece (z ¼ x ¼ 0) along the y axis are shown in Fig. 6. According to Fig. 6a, the outer edge of the shoulder, where the

velocity is highest, is where the strain rate reaches its maximum value. At the AS and RS, the maximum strain rates are 975 s^-1 and 926 s^-1, respectively. The strain rates reach their maximum at y ¼ 0.006 m. The same points (y ¼ 0.006 m) yield the peak temperatures, as shown in Fig. 3.Thus, the higher temperatures are a result of the higher strain rates. Nandan et al. [14] and Kishore et al. [15] reported a similar outcome. These results are in good agreement with the values obtained in other simulation works [37]. Because the shear rate is highest at the AS, peak strain rate attains at this side.

The variations of viscosity, which expressed as a logarithm tobase 10, is inversely related to the strain rate, as shown in Fig. 6b.The maximum values of viscosity are obtained on the pin surface where the strain rate is minimum. When the viscosity reaches 106 at the y ¼ 0.008m on the AS (Al-Mg2Si composite) and 107 at the y¼0.008m on the RS (AA6061 aluminum alloy), no more plastic flow occurs. At these points, which are close to the edge of the shoulder, the strain rate reaches to zero and the materials do not expose to more plastic deformation. Actually the deformed area is limited under the shoulder. The deformed area (nugget) will be shown in the macrographs and discussed more latter.The strain rate contours at a vertical plane out of the pin surface(x ¼ 0.0026m> Rp) is shown in Fig. 7. The strain rate is Maximumat the interface of the workpiece and the shoulder and decreaseswith increasing the distance from the top surface. This is because of the effect of the tool shoulder as a source of momentum at the top
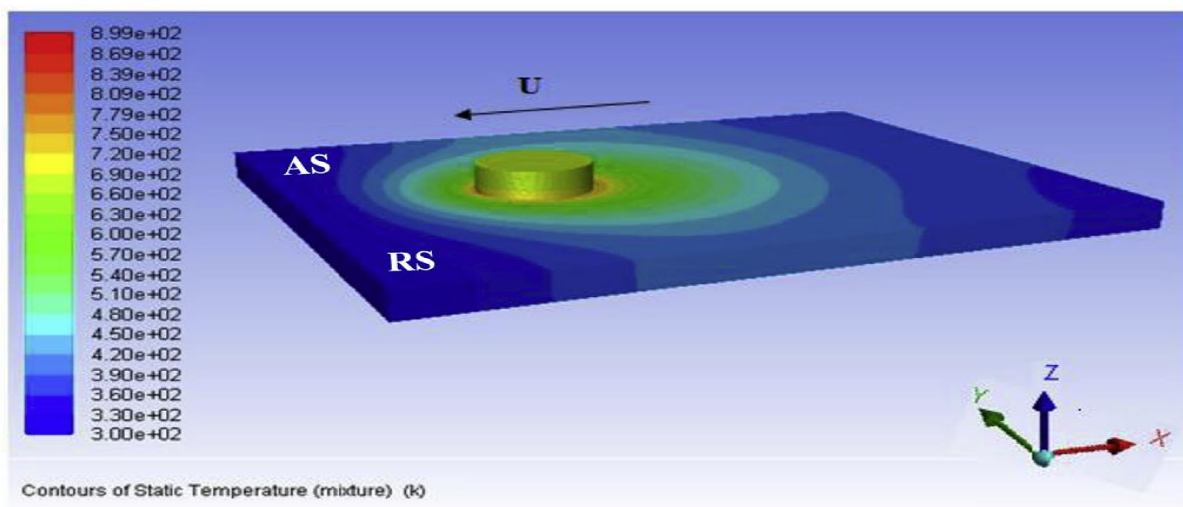

Fig. 2. 3D temperature distribution at the rotational speed of 1120 rpm and welding velocity of 0.002 m/s.

The material flow stream lines surrounding the pin at a welding speed of 0.002 m/s and a rotational speed of 1120 rpm are shown in Fig. 8. It is consistent with the presence of a circulating plasticized layer of material close to the tool pin for the stream lines depict the 2D circular and closed flow of material around the tool pin. The circular tool motion pattern produces the circular stream lines.The materials travel around the tool and enter between AS and the leading edge before leaving. Between AS and the trailing side is where the materials exit [38]. The primary material flow occurs on the RS, which is home to the aluminum alloy AA6061. The primary material flow occurs on the RS, which is also home to the aluminum alloy AA6061. This is in good accord with the findings of Colligan [39] and Padmanaban et al. [16]. Figure 9 shows the simulated volume fraction distributions and cross-section macrographs at the three rotational speeds. There are no flaws or imperfections in the FSW joints, such as voids or tunnels. The following explanation applies to the material flow pattern: The Al-Mg2Si composite is mixed together at the RS after turning with the tool pin at the AS. After that, the last bonding occurs [40].

The SZ macrostructure can be split into two regions based on the experimental cross-sections: region A, which is dominated by dynamic recrystallization, and region B, which is dominated by material mixing. The region A is visible on the RS but invisible on the AS, as seen in Fig. 9a. This is most likely due to the fact that AA6061 alloy experiences dynamic recrystallization more frequently than Al2Mg composite. As a result, as shown in Fig. 9, the SZ can be assumed to be between the volume fraction of 0 (blue area) and 1 (red area). Al-Mg2Si composite and AA6061 alloy are shown by the blue and red regions, respectively.

In the predicted SZs, the region B can be corresponded to the area where the volume fraction is between 0.4 and 0.8. Also, the region A corresponds to the area where the volume fraction is more than 0.8 and less than 0.4.The formation of the SZ is caused by two material flow modes: (i) pin flow and (ii) shoulder flow [41, 42]. In both the experimental and predicted SZs, the shoulder flow region on the RS is larger than that on the AS. The comparable outcome documented in scholarly works [10]. It is anticipated that the shoulder flow region's width will be greater than the pin flow region's width. In both the predicted and experimental SZs, the shoulder flow region's width is greater on the RS. On the other hand, the AS shows nearly equal shoulder and pin flow region widths, and both the experimental and predicted SZ boundaries are straight. This maximum volume fraction is found on the upper SZ. Instead

All experimental SZs of the samples exhibit the stacked layer pattern (serrated interface), which becomes more pronounced at rotational speeds of 720 and 1120 rpm (Fig. 9a and c). The rotational speed increases from 720 to 1120 rpm as the number of layers (serrates) increases from three to five. This pattern is identified in the predicted SZs at rotational speeds of 1120 and 720 rpm, but not at 920 rpm (Fig. 9b). In every sample, the materials have been appropriately mixed together. At 920 rpm, the mixing is more intense, though. Because of this, the volume fraction contours allow us to predict the shape of the SZ or nugget. The weld cross-section macrographs and the predicted SZ are in agreement. It can be very helpful in forecasting the properties of welds and minimizes the amount of necessary experimental testing.
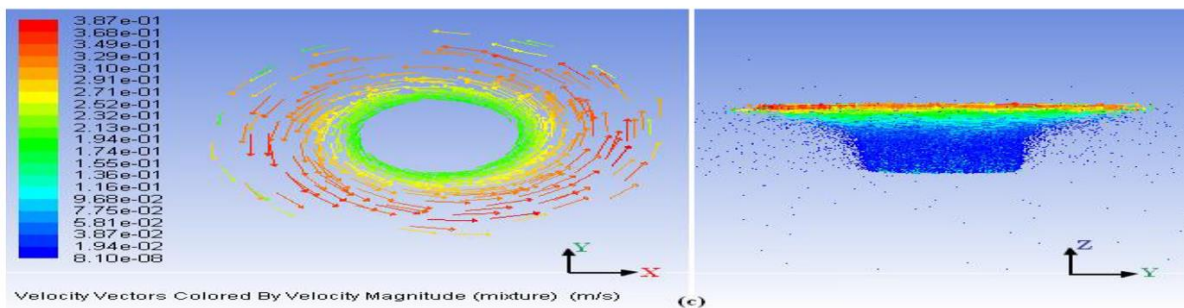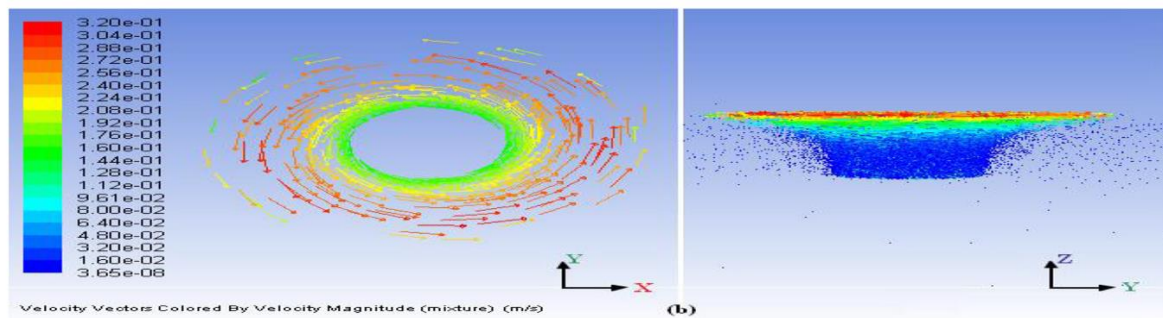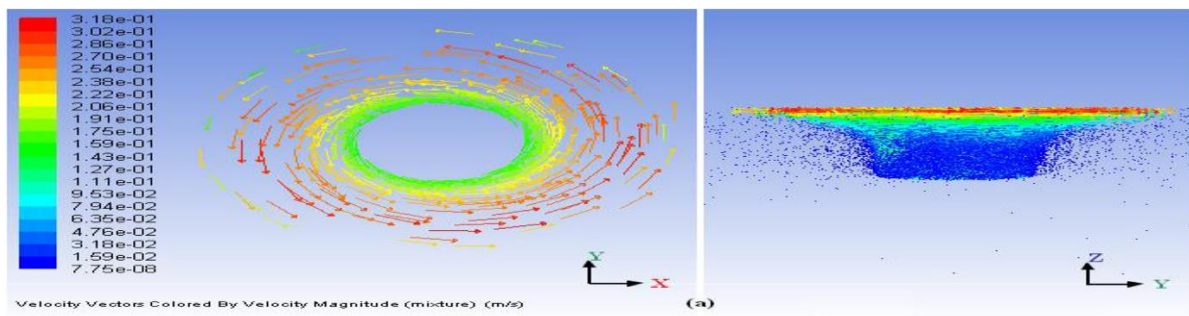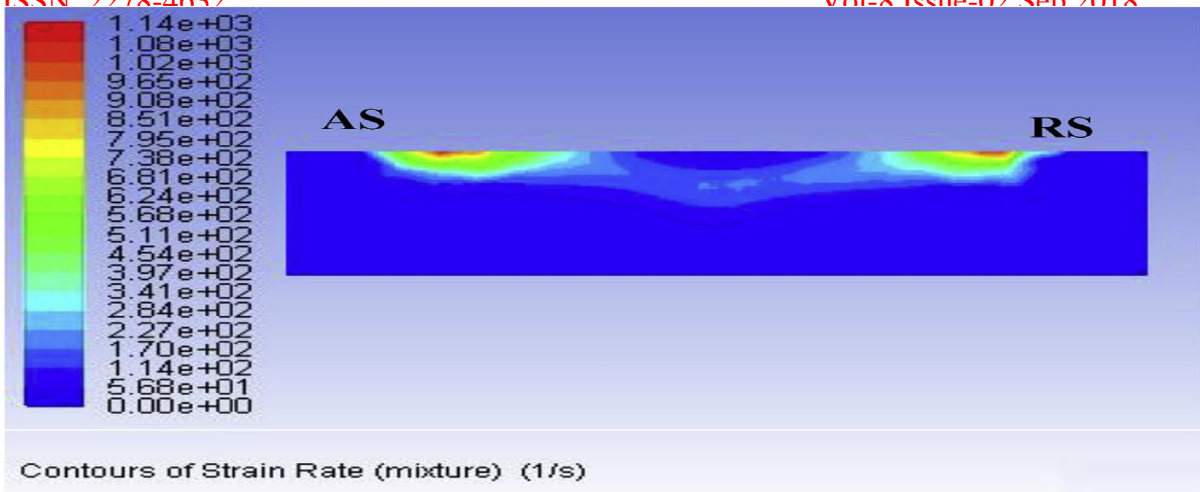
Fig. 7. Contours of strain rate at the vertical plane out of the pin (x ¼ 0.0026). Thewelding velocity is 0.002 m/s and the rotational speed is 1120 rpm.
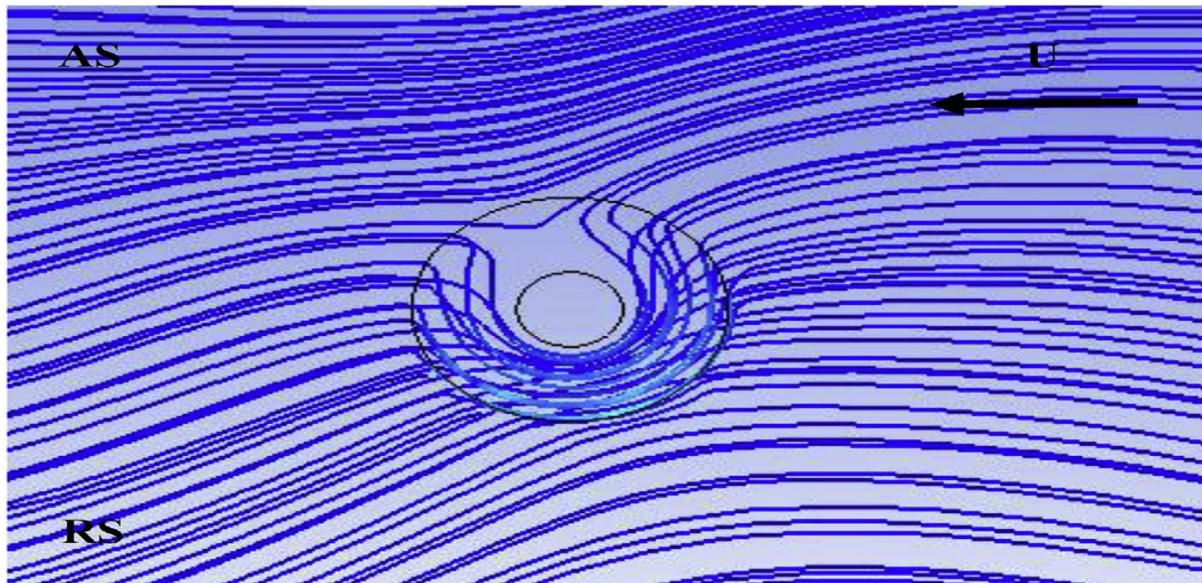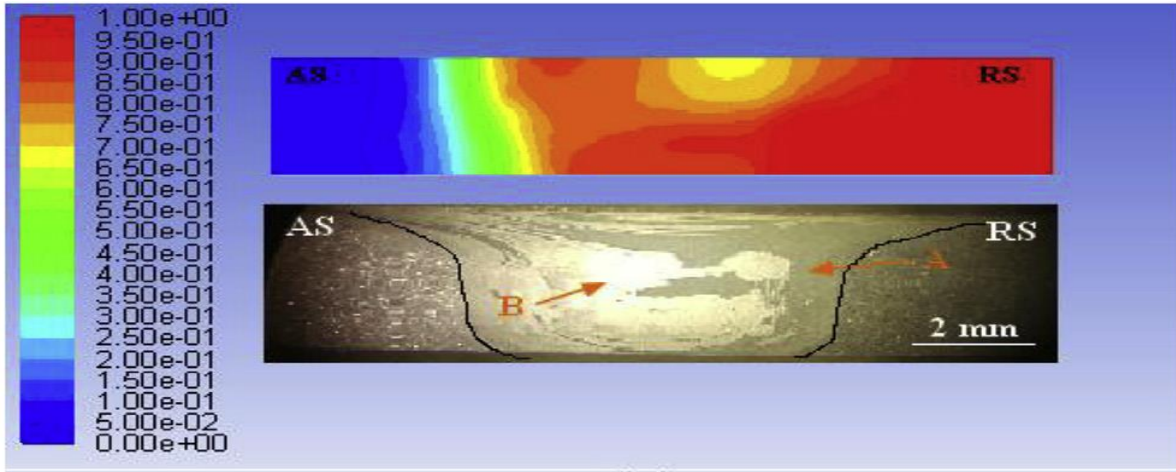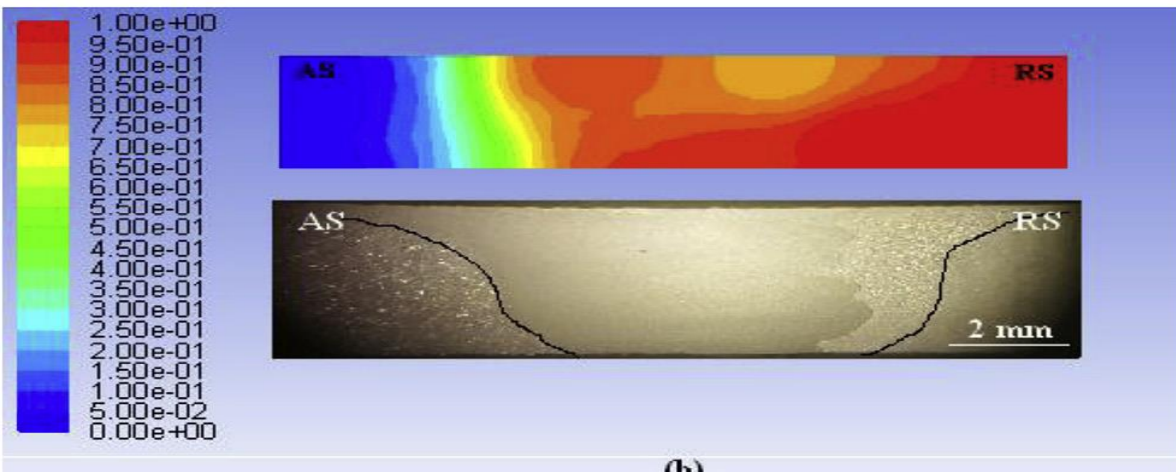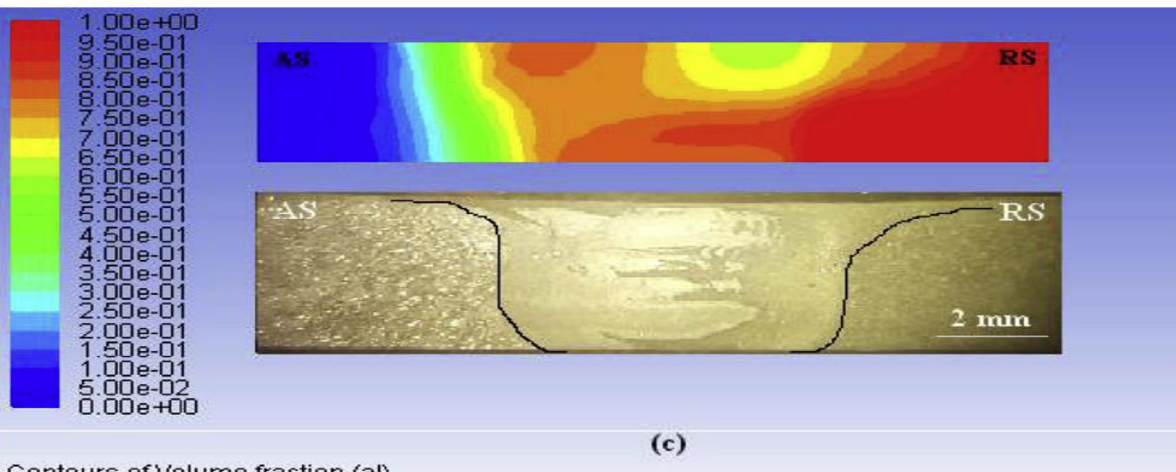

Fig. 8. Material flow pattern around the tool pin. The welding velocity is 0.002 m/s and the rotational speed is 1120 rpm.

Contours of Volume fraction (al)

(a)

Contours of Volume fraction (al)

(b)

Contours of Volume fraction (al)

(c)

Fig. 9. vol fraction fields of AA6061 aluminum alloy and corresponding weld macrographs at cross section of workpiece. The welding velocity is 0.002 m/s. The rotational speed is a) 720 rpm, b) 920 rpm, c) 1120 rpm.

5. Conclusions

In this study, strain rate, material flow, and nugget shape during dissimilar FSW of Al-Mg2Si composite and AA6061 aluminum alloy are investigated using a three-dimensional CFD-based model. The model took into account the volumetric heat generation and the volume of fluid (VOF) method. The following is an expression of the study's findings:

1 The SZ shape is predictable through the simulated volume fraction contours. The predicted SZs agree with the experimental macrographs.

2.At the rotational speed of 1120 rpm and the welding velocity of 0.002 m/s, the peak temperature and maximum strain rate are 887 K and 975 s_1, which occurs at the AS, respectively.

3 The variation of the viscosity is opposed to the strain rate and the amount of plastic deformation reduces with increasing of the viscosity.

4 The SZ can be divided to two regions: (i) The region where dynamic recrystallization is dominant and the volume fraction is less than 0.4 and more than 0.8, and (ii) the region where the material mixing is dominant and the volume fraction is in the range of 0.4e0.8.

References

[1] K.-S. Bang, K.-J. Lee, H.-S. Bang, H.-S. Bang, Interfacial microstructure a mechanical properties of dissimilar friction stir welds between 6061-T6 aluminum and Ti-6%Al-4%V alloys, Mater. Trans. 52 (5) (2011) 974e978.

[2] A. Jahangiri, M.H. Idris, S. Farahany, Investigation on tungsten inert gas welding of in situ Al-15 and 20 Mg2Si composites with an Al-Si filler, J. Compos. Mater. 47 (10) (2012) 1283e1291.

[3] H.R. Jafari Nodooshan, W. Liu, G. Wu, A. Bahrami, M.I. Pech-Canul, M. Emamy,Mechanical and tribological characterization of Al-Mg2Si composites after yttrium addition and heat treatment, J. Mater. Eng. Perform. 23 (4) (2014) 1146e1156.

[4] K. Elangovan, V. Balasubramanian, S. Babu, Predicting tensile strength of friction stir welded AA6061 aluminium alloy joints by a mathematical model, Mater. Des. 30 (2009) 188e193.

[5] M. Sharifitabar, H. Nami, Microstructures of dissimilar friction stir welded joints between 2024-T4 aluminum alloy and Al/Mg2Si metal matrix cast composite, Compos. Part B Eng. 42 (7) (2011) 2004e2012.

[6] I. Dinaharan, N. Murugan, Automation of friction stir welding process to join aluminum matrix composites by optimization, Proc. Eng. 38 (2012) 105e110.

[7] A. Farzadi, M. Bahmani, D.F. Haghshenas, Optimization of operational parameters in friction stir welding of AA7075-T6 aluminum alloy using response surface method, Arab. J. Sci. Eng. 42 (11) (2017) 4905e4916.

[8] I. Shigematsu, Y.J. Kwon, K. Suzuki, T. Imai, N. Saito, Joining of 5083 and 6061 aluminium alloys by friction stir welding, J. Mater. Sci. Lett. 22 (2003) 353e356.

[9] J.A. Wert, Microstructures of friction stir weld joints between an aluminiumbase metal matrix composite and a monolithic aluminium alloy, Scr. Mater. 49 (6) (2003) 607e612.

[10] Y. Huang, Y. Wang, L. Wan, H. Liu, J. Shen, Material-flow behavior during friction-stir welding of 6082-T6 aluminum alloy, Int. J. Adv. Manuf. Technol. 87 (2016) 1115e1123.

[11] A.A.M. Silva, E. Arruti, G. Janeiro, E. Aldanondo, P. Alvarez, A. Echeverria, Material flow and mechanical behaviour of dissimilar AA2024-T3 and AA7075-T6 aluminium alloys friction stir welds, Mater. Des. 32 (4) (2011) 2021e2027.

[12] P. Alvarez, G. Janeiro, A.A.M. Silva, E. Aldanondo, A. Echeverrı, Material flow and mixing patterns during dissimilar FSW, Sci. Technol. Weld. Join. 15 (8) (2010) 648e653.

[13] D. Kim, et al., Numerical simulation of friction stir butt welding process for AA5083-H18 sheets, Eur. J. Mech. A/Solids 29 (2) (2010) 204e215.

[14] R. Nandan, G.G. Roy, T.J. Lienert, T. DebRoy, Numerical modelling of 3D plastic flow and heat transfer during friction stir welding of stainless steel, Sci. Technol. Weld. Join. 11 (5) (2006) 526e537.

[15] V.R. Kishore, J. Arun, R. Padmanabhan, V. Balasubramanian, Parametric studies

of dissimilar friction stir welding using computational fluid dynamics simulation, Int. J. Adv. Manuf. Technol. 80 (1e4) (2015) 91e98.

[16] R. Padmanaban, V. Ratna Kishore, V. Balusamy, Numerical simulation of temperature distribution and material flow during friction stir welding of dissimilar aluminum alloys, Proc. Eng. 97 (2014) 854e863.

[17] X. Liu, G. Chen, J. Ni, Z. Feng, Computational fluid dynamics modeling on steady-state friction stir welding of aluminum alloy 6061 to TRIP steel, J. Manuf. Sci. Eng. 139 (2017), 051004.

[18] H.A. Derazkola, M. Elyasi, M. Hosseinzadeh, CFD modeling of friction stir welding of AA1100 aluminum alloy to A441 AISI steel butt joint, J. Adv. Mater. Process. 3 (3) (2015) 47e59.

[19] H. Jamshidi Aval, S. Serajzadeh, A.H. Kokabi, Thermo-mechanical and microstructural

issues in dissimilar friction stir welding of AA5086-AA6061, J. Mater. Sci. 46 (10) (2011) 3258e3268.

[20] H. Wang, Numerical and artificial neural network modelling of friction stir welding, Sch. Appl. Sci. (2011) 2007e2011 (November).

[21] G. Yoshikawa, F. Miyasaka, Y. Hirata, Y. Katayama, T. Fuse, Development of numerical simulation model for FSW employing particle method, Sci. Technol. Weld. Join. 17 (4) (2012) 255e264.

[22] R. Nandan, T. Debroy, H.K.D.H. Bhadeshia, Recent advances in friction-stir welding e process, weldment structure and properties, Prog. Mater. Sci. 53 (2008) 980e1023.

[23] R. Nandan, G.G. Roy, T. Debroy, Numerical simulation of three-dimensional heat transfer and plastic flow during friction stir welding, Metall. Mater.

Trans. A 37A (2005) 1247e1259.

[24] R. Nandan, G.G. Roy, T.J. Lienert, T. Debroy, Three-dimensional heat and material

flow during friction stir welding of mild steel, Acta Mater. 55 (3) (2007) 883e895.

[25] C.M. Sellars, W.J.M. Tegart, Hot workability, Int. Metall. Rev 17 (1972) 1e24.

[26] T. Sheppard, D.S. Wright, Determination of flow stress: part 1 constitutive equation for aluminium alloys at elevated temperatures, Metal Technol. (june, 1979) 215e223.

[27] P.A. Colegrove, H.R. Shercliff, CFD modelling of friction stir welding of thick plate 7449 aluminium alloy, Sci. Technol. Weld. Join. 11 (4) (2006) 429e441.

[28] C.S. Wu, W. Bin Zhang, L. Shi, M.A. Chen, Visualization and simulation of plastic material flow in friction stir welding of 2024 aluminium alloy plates, Trans. Nonferrous Met. Soc. China Eng. Ed. 22 (6) (2012) 1445e1451.

[29] C. Hamilton, S. Dymek, A. Sommers, A thermal model of friction stir welding in aluminum alloys, Int. J. Mach. Tools Manuf 48 (10) (2008) 1120e1130.

[30] J. Zhang, Z. Fan, Y. Wang, B. Zhou, Microstructure and mechanical properties of in situ Al - Mg2Si composites, Mater. Sci. Technol 16 (2000) 913e918.

[31] P.A. Colegrove, H.R. Shercliff, 3-Dimensional CFD modelling of flow round a threaded friction stir welding tool profile, J. Mater. Process. Technol. 169 (2) (2005) 320e327.

[32] A.P. Reynolds, M.Z.H. Khandkar, J.A. Khan, A.P. Reynolds, Prediction of temperature distribution and thermal history during friction stir welding : input torque based model prediction of temperature distribution and thermal history during friction stir welding : input torque based model, Sci. Technol. Weld. Join 8 (3) (2003) 165e174.

[33] A.K. Lakshminarayanan, V. Balasubramanian, Process parameters optimization for friction stir welding of RDE-40 aluminium alloy using Taguchi technique Trans. Nonferrous Met. Soc.China 18 (2008) 548e554.

[34] B. Wang, B. Lei, J. Zhu, Q. Feng, L. Wang, D. Wu, EBSD study on microstructure and texture of friction stir welded AA5052-O and AA6061-T6 dissimilar joint, JMADE 87 (2015) 593e599.

[35] M. Khethier, A. Sabah, K. Hussein, A. Adnan, Optimization of mechanical properties of friction stir spot welded joints for dissimilar aluminum alloys (AA2024-T3 and AA 5754-H114), Arab. J. Sci. Eng. 41 (2016) 4563e4572.

[36] A. Farzadi, Correlation between precipitate microstructure and mechanical properties in AA7075-T6 aluminum alloy friction stir welded joints, Mat.- Wiss. u. Werkstofftech. 48 (2) (2017) 151e162.

[37] H. Wang, P.A. Colegrove, F. Jorge, Numerical investigation of the tool contact condition during friction stir welding of aerospace aluminium alloy, Comput. Mater. Sci. 71 (2013) 101e108.

[38] R. Kumar, V. Pancholi, R.P. Bharti, Material fl ow visualization and determination

of strain rate during friction stir welding, J. Mater. Process. Tech. 255 (July 2017) 470e476.

[39] K. Colligan, Material flow behavior during friction stir welding of aluminum, Weld. Res. Suppl. (1999) 229e237.

[40] G. Buffa, M. De Lisi, A. Barcellona, L. Fratini, Material flow analysis in dissimilar friction stir welding of AA2024 and Ti6Al4V butt joints, in: MATEC Web of Conferences, 2016.

[41] R.M. Leal, C. Leit~ao, A. Loureiro, D.M. Rodrigues, P. Vilac, Material flow in heterogeneous friction stir welding of thin aluminium sheets: effect of shoulder geometry, Mater. Sci. Eng. A 498 (2008) 384e391.

[42] K. Kumar, S.V. Kailas, The role of friction stir welding tool on material flow and weld formation, Mater. Sci. Eng. A 485 (2008) 367e374.